NeuroImage 237 (2021) 118131

Contents lists available at ScienceDirect

NeuroImage

journal homepage: www.elsevier.com/locate/neuroimage

Working memory task induced neural activation: A simultaneous PET/fMRI study

Isabelle Ripp[a,c,d,1,*], Lara A Wallenwein[a,1], Qiong Wu[b,c,e], Monica Emch[b,c,d], Kathrin Koch[b,c,d], Paul Cumming[f,g], Igor Yakushev[a,c,d]

[a] Department of Nuclear Medicine, School of Medicine, Klinikum Rechts der Isar, Technical University of Munich, Munich, Germany
[b] Department of Neuroradiology, School of Medicine, Klinikum Rechts der Isar, Technical University of Munich, Munich, Germany
[c] TUM-Neuroimaging Center (TUM-NIC), Technical University of Munich, Munich, Germany
[d] Graduate School of Systemic Neurosciences, Ludwig-Maximilians-Universität, Martinsried, Germany
[e] Institute of Medical Psychology, Ludwig-Maximilians-Universität, Munich, Germany
[f] Department of Nuclear Medicine, University Hospital Bern, Bern, Switzerland
[g] School of Psychology and Counselling, Queensland University of Technology, Brisbane, Australia

ARTICLE INFO

Keywords:
Cognition
FDG PET
fMRI
Neuroimaging
Positron emission tomography

ABSTRACT

Purpose: Positron emission tomography (PET) with [^{18}F]fluorodeoxyglucose (FDG) is a powerful method for mapping cerebral glucose metabolism as a proxy of neural activity, assuming a steady-state during the recording interval. We asked if a clinical FDG-PET imaging protocol might also capture changes in neural activity associated with performance of a working memory (WM) task.

Methods: To test this concept, we examined hybrid PET/MR data for FDG-PET and simultaneous functional magnetic resonance imaging (fMRI) in a sample of healthy volunteers. The PET image acquisition started 30 min after a bolus injection of approximately 100 MBq FDG, and the WM task was undertaken starting at approximately 60 min post-injection. We reconstructed FDG-PET sum images corresponding to baseline (44–60 min p.i.) and WM tasks (63- 71 min p.i.), each with intensity scaling to the corresponding global mean.

Results: Compared to the baseline resting condition, relative FDG uptake increased during WM task performance in brain regions previously associated with WM. Furthermore, these metabolically active regions partly overlapped with the regions showing task-dependent increases in BOLD signal in simultaneous fMRI.

Conclusion: We find evidence for WM task-induced neural activation using a clinical FDG-PET imaging protocol. These findings encourage the development of dedicated protocols for tracking neural correlates of cognitive function.

Introduction

Under physiological conditions, glucose is the major substrate for brain energy metabolism. As such, positron emission tomography (PET) with the glucose analogue [^{18}F]fluorodeoxyglucose (FDG) has proven immensely useful for the study of neuroenergetics in the living human brain, both in clinical and research settings (Bohnen et al., 2012; Riedl et al., 2016). While the cerebral FDG trapping that occurs during a given PET recording interval is generally indicative of the mean cerebrometabolic activity during the preceding interval of tracer circulation, there is also scope for measuring transient changes in metabolism using functional FDG-PET (Verger and Guedj, 2018; Villien et al., 2014). In the continuous infusion paradigm, the slope of the cerebral FDG uptake as a function of infusion time is supposed to give an instantaneous index of cerebral metabolic activity, which can capture neural correlates of visual stimulation or performance of a simple motor task during a single recording session (Hahn et al., 2016; Jamadar et al., 2019a; Rischka et al., 2018). Alternately, FDG-PET activation studies can entail the comparison of two scanning sessions, usually recorded on separate days (Siebner et al., 2000).

The main cerebral uptake occurs during the initial 30 min post injection (p.i.) of the bolus, during which time the plasma FDG concentration declines by some 75% (Huang et al., 1980). However, about 7% of the original plasma radioactivity remains at 60 min after a bolus injection. It follows that cerebral trapping continues at an ever-diminishing rate, in parallel with the declining arterial input function. Indeed, the brain

* Corresponding author: Department of Nuclear Medicine, Technical University of Munich, Ismaninger Str. 22, 81675 Munich
E-mail address: isabelle.ripp@tum.de (I. Ripp).
[1] These authors contributed equally to this work.

https://doi.org/10.1016/j.neuroimage.2021.118131.
Received 20 January 2021; Received in revised form 1 April 2021; Accepted 28 April 2021
Available online 2 May 2021.

radioactivity concentration peaks at 90 min p.i. (Jamadar et al., 2019b; Phelps et al., 1979) and declines slowly thereafter due to the progressive effect of slow dephosphorylation of FDG-phosphate in brain, which occurs at a rate one tenth that of the hexokinase reaction (Huang et al., 1980). This phenomenon gives some scope for detecting increases in cerebral glucose utilization in the context of an ordinary bolus injection paradigm. Thus, Ishii et al. (Ishii et al., 2006, 2002) found highly significant increases in net FDG uptake in the 60 min p.i. frame compared to the frame at 30 min p.i., which might well be sensitive to cognitive activation during that late interval.

The aim of this study was to test if PET with a single bolus injection of FDG, in the context of a clinical imaging protocol, can detect increases in neural activity due to a working memory (WM) task. To this end, we used a hybrid PET/MR scanner to obtain simultaneous blood-oxygen-level-dependent (BOLD) signal and FDG-uptake recordings in healthy volunteers before and during performance of a WM task. Indeed, BOLD-fMRI is currently the most popular imaging modality to capture task-related brain activation. As compared to FDG PET, it possesses a higher temporal resolution, is cheaper and devoid of radiation exposure. However, FDG-PET provides a higher signal-to-noise ratio and, most importantly, it measures neural or synaptic activity in a more direct way, by estimating glucose utilization via neurometabolic coupling (Magistretti and Allaman, 2015). In contrast, BOLD-fMRI relies on so called neurovascular coupling, a complex interaction between regional cerebral blood volume, flow, and metabolic rate of oxygen (Kim and Ogawa, 2012).

Materials and methods

The data used in this study are drawn from a prospective investigation of transfer effects and neural substrates of WM training in healthy middle-aged volunteers. The participants underwent an adaptive or non-adaptive 8-week training between two PET/MRI scanning sessions after their assignment to an experimental or an active control group, respectively. The results of that study shall be published separately. The Federal Office for Radiation Protection and the Ethical Committee of the Klinikum Rechts der Isar, Technical University of Munich approved the transfer effects study.

Participants

Participants were recruited via advertisement in the internet and a hospital bulletin board. Only healthy, right-handed, German-speaking individuals aged 50 to 65 years were included. The exclusion criteria were self-reported or objective (on test battery) cognitive deficits, history of a neurological or psychiatric disease, contraindications for MRI, and relevant anomalies on structural MRI images. Prior to entry, participants were informed about the aims, expected advantages, and potential risks of the study upon consideration, and then gave their written, informed consent. A *post hoc* detected triggering failure caused a delay of the first task relative to the preceding resting state in 7 subjects. Their PET data had to be excluded from the subsequent analyses, along with PET data of further 7 subjects, whose data were acquired incompletely. Thus, the available sample for PET analyses consisted of 49 participants (24 female) with a mean age of 55.7 years (SD = 4.1). For the fMRI analyses, 6 participants had to be excluded due to extensive movement of more than 3 mm or 3° maximum displacement during scanning and one due to a failure in spatial normalization, resulting in a sample of 56 participants (28 female) with a mean age of 55.7 years (SD = 4.2). Out of the included data sets, both PET and fMRI data were available for 42 subjects.

We were interested in a spatial effect of activation due to task performance, while a possible influence of WM training was of no relevance. Therefore, the data of both training groups and both scanning sessions were pooled for the present study.

Data acquisition

The participants underwent two PET/MR imaging sessions, one before and one after WM training. The PET and MRI data were acquired simultaneously on a hybrid (3 T) PET/MRI Siemens Biograph mMR scanner with a vendor-supplied 16-channel head coil and placement of cushions to minimize head movement. Participants had been instructed to fast for six hours prior to neuroimaging, and their blood glucose level was confirmed to be < 150 mg/dl at the time of FDG administration (mean = 94.23 mg/dl; SD = 9.62; range = 52–122 mg/dl). Participants sat comfortably in a quiet, dimly lit room before intravenous injection of approximately 100 MBq of FDG as a slow bolus. Given that the participants were healthy subjects to be subjected to two PET/MRI sessions, this comparatively low dose of FDG was chosen to reduce radiation exposure. This decision is supported by an approximately 1.6 times higher sensitivity of our PET/MR system as compared to its PET/CT counterpart (Delso et al., 2011). The participants were instructed not to speak, read, or walk during the initial uptake period of at least 10 min, and then entered the tomograph for acquisition of emission data from 30 to 90 min p.i. in list mode.

During the PET scanning session, high-resolution T1-weighted images were acquired using a three-dimensional (3D) normal gradient recalled sequence with the following parameters: 160 slices, time of repetition (TR) = 2300 ms, echo time (TE) = 2.98 ms, flip angle = 9.0°, FOV = 256 mm, bandwidth: 240 Hz/Px, matrix size = 256 × 240 mm, slice thickness = 1 mm (no gap), voxel size of 1.0 × 1.0 × 1.0 mm^3, interleaved acquisition. Prior to the resting state functional MRI (fMRI) acquisition, participants were instructed to close their eyes, stay awake, and think of nothing in particular. Subsequently, a T2*-weighted EPI-Prospective Acquisition CorrEction sequence for task fMRI was acquired with the following parameters: 237 slices, TR = 2700 ms, TE = 30 ms, flip angle = 90°, FOV = 192 mm, bandwidth= 2232 Hz/Px, matrix size 192×144 mm, slice thickness = 3 mm (0.6 mm gap), voxel size = 3.0 × 3.0 × 3.0 mm^3, interleaved acquisition.

Working memory task

During the task fMRI sequence, participants performed a visual and verbal version of the *n*-back task (Jaeggi et al., 2010). Task order of the visual and verbal tasks was counterbalanced between the first and second scanning days. Each task consisted of seven blocks of an active condition (3-back for verbal and 2-back for visual) and seven blocks of a control X-back condition. The X-back condition is a purely attentional task, in which participants have to press a button whenever a specific shape (visual task) or the letter “X” (verbal task) is presented. The verbal task included one more n-back level than the visual one, as subjects are assumed to be more familiar with letters than abstract shapes. Each condition lasted 45 s, including five seconds of an oral instruction in German language, five seconds of fixation cross presentation, and 35 s of stimulus presentation (Fig. 1). Thus, each WM task lasted 10.5 min.

Image data pre-processing

PET image reconstruction was performed offline using Siemens e7 Tools (Siemens Molecular Imaging, Knoxville, USA) via an ordered subsets expectation maximization algorithm with 24 subsets and 3 iterations. A 5 mm Gaussian filter was used to eliminate high frequency noise. The resulting images consisted of 127 sagittal slices with matrix dimensions of 344×344 and a voxel size of 1.04 × 1.04 × 2.03 mm^3. An ultra-short time echo μ-map with 300 sagittal slices, matrix dimensions of 300×300 and voxel size of 1.6 × 1.6 × 1.6 mm^3 was used to perform MR attenuation correction based on tissue segmentation.

Four serial summation PET images were reconstructed, each lasting 7.8 min, as depicted in Fig. 2. The resting state PET frames were recorded at 44–52 min (Rest1) and 52–60 min (Rest2). The latter frame

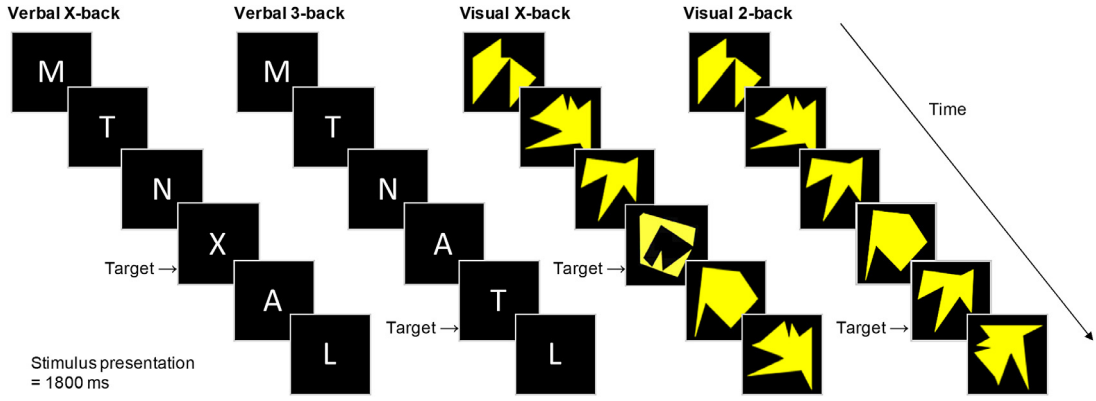

Fig. 1. Example of n-back conditions as used in the scanning task paradigm.

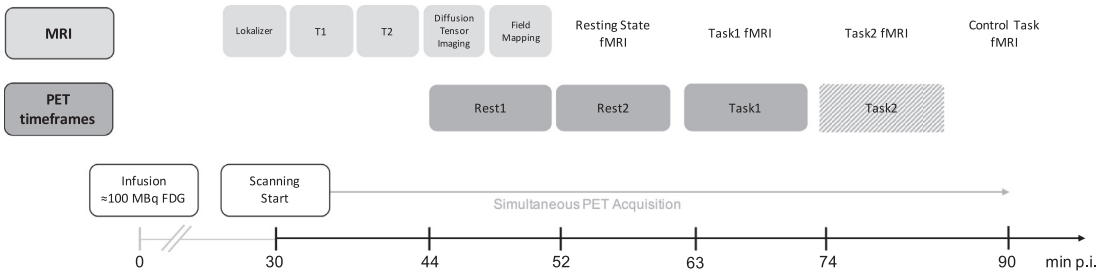

Fig. 2. PET/MR scanning timeline. MRI sequences and corresponding PET timeframes

was coincident with the resting state fMRI sequence. The third PET frame (Task1) was recorded at 63–71 min, during performance of the first WM task, and the fourth frame (Task2) was recorded at 74–81 min p.i., during performance of the second WM task. We confined our present activation analysis to the first task frame (Task1), which was obtained in counterbalanced order of the visual and verbal WM tasks. Thus, Task1 reflects the composite of neural activity underlying the visual and verbal WM tasks, which we treat for the present as a single WM activation state, given that they both engage the same core network (Owen et al., 2005; Rottschy et al., 2012). Although used for preprocessing, the second WM task was not included in the analyses, as it represents an accumulated signal from Task1 and Task2 and is therefore difficult to interpret. Correspondingly, we included only the data of the first task fMRI block in the analyses.

Image preprocessing and analysis were performed using SPM12 (https://www.fil.ion.ucl.ac.uk/spm/software/spm12) in MATLAB v2018b (The MathWorks, Inc., Natick, Massachusetts, USA). First, individual Rest1, Rest2, and Task1 PET images were realigned to the mean of the four frames, followed by co-registration to the corresponding individual T1-weighted image. For both coregistration of PET to T1 and for spatial normalization into the MNI space a 4th degree B-Spline interpolation was applied. Individual T1-weighted images were then aligned to the MNI space to obtain a forward deformation matrix, which was subsequently applied to the PET images, followed by smoothing with an 8 mm Gaussian filter. The fMRI images were realigned to the mean fMRI image to correct for head motion and then co-registered to the corresponding T1-weighted image using normalized mutual information. We used a 3 mm maximum displacement as a movement threshold. The co-registered fMRI images were then aligned to the MNI space, followed by smoothing with an 8 mm Gaussian filter. Visual quality checks were performed to ensure accurate co-registration and normalization.

Statistical analyses

For PET data, a 2 × 3 repeated measures analysis of variance (ANOVA) with scanning session (days 1 and 2) and time frame (Rest1, Rest2 and Task1) as within-subject factors was conducted in SPM with the following (default) settings: grand mean scaling, global calculation using global mean *within each image* for normalization, and overall grand mean scaling to the factor 50. This approach was chosen to adjust for the known increase in whole brain FDG uptake over time (Ishii et al., 2006). Furthermore, an explicit mask and a relative intensity threshold of 0.8 were applied to exclude extracerebral FDG uptake (e.g. ocular muscles). The explicit mask was calculated using individual gray and white matter probability maps obtained from the segmentation of individual T1-weighted images in the MNI space. A voxel was included if its mean probability of belonging to gray or white matter (over all participants) exceeded 20% (Dukart and Bertolino, 2014). As no differences between the two sessions were found (data not shown), the contrast "Task1 > Rest2" was computed over both sessions. A probability threshold of $p < .05$ family-wise error (FWE) corrected for multiple comparisons at a voxel-level and a threshold for spatial extent of at least 30 contiguous voxels were applied. Apart from time, or frame specific, global normalization, an additional analysis was performed to adjust for time-dependent changes in FDG uptake in a more conservative fashion. Specifically, we computed a contrast of contrasts, i.e. Task1 > Rest2 versus Rest2 > Rest1 (Supplemental Figure 2 and Supplemental Table 5).

For analysis of task fMRI, we applied a general linear model on the first level. Six motion parameters were included as covariates of no interest. Aiming to make the fMRI analysis more comparable to the PET analysis, we contrasted each condition against the implicit baseline, resulting in separate contrast images for visual X-back, visual 2-back, verbal X-back and verbal 3-back for each participant. On the second level, we

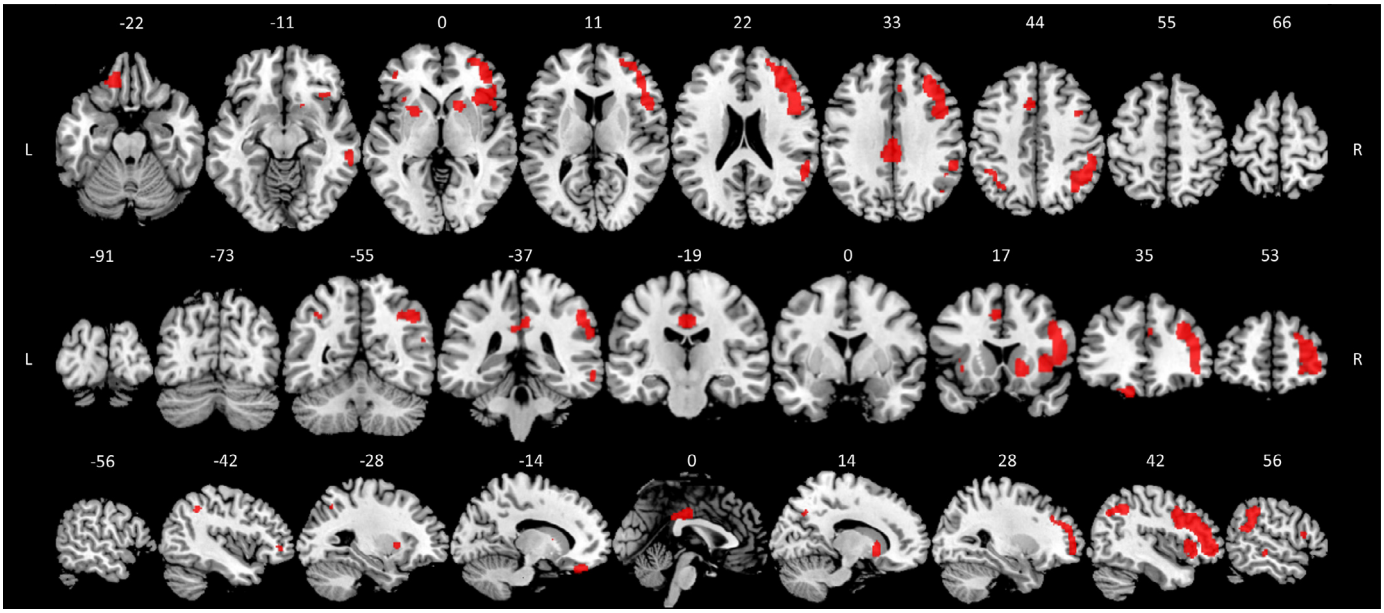

Fig. 3. Higher globally normalized FDG uptake during a working memory task compared to the preceding resting state. Whole-brain repeated measures ANOVA of PET data for Task1 > Rest2 over both sessions with p < .05 family-wise error correction and cluster extent ≥ 30 voxels. L = left; R = right.

Table 1
List of brain regions showing higher relative FDG uptake during a working memory task compared to a preceding resting state.

Region	Cluster Extent	Peak Coordinate MNI (x y z)	T-value (df = 288)
R. Putamen	205	16 14 −4	9.44
L. Orbitofrontal cortex	143	−16 38 −26	8.96
R. Supramarginal gyrus (extending into R. Angular gyrus)	976	46 −50 42	8.26
R. Middle cingulate cortex (extending to L. Middle & Posterior cingulate cortex)	431	0 −22 36	7.88
R. Middle frontal gyrus (extending into R. Inferior frontal gyrus, Dorsolateral prefrontal cortex, and R. Insula)	3421	40 26 30	7.81
L. Putamen	214	−24 8 0	6.44
R. Middle temporal gyrus	132	62 −38 −10	6.05
L. Dorsal anterior cingulate cortex (extending into L. Supplementary motor area)	89	−6 14 42	6.05
R. Precuneus	62	10 −64 38	5.76
L. Inferior parietal gyrus	144	−46 −48 40	5.73
R. Dorsal anterior cingulate cortex	53	6 30 34	5.29
L. Middle frontal gyrus	30	−40 46 −4	5.25

Whole-brain repeated measures ANOVA for Task1 > Rest2 over both sessions with $p < .05$ family-wise error correction, cluster extent ≥ 30 voxels.
L = left; *R* = right; MNI = Montreal Neurological Institute space coordinates; df = degrees of freedom.

applied repeated measures ANOVAs with the within-subject factor task condition (active and control) separately for the visual and verbal task. We again contrasted the four conditions individually to obtain group level activations for each condition. We applied a probability threshold of $p < .05$ FWE corrected for multiple comparisons at a voxel-level and a threshold for spatial extent of at least 30 contiguous voxels. Subsequently, we calculated a summed image depicting the net voxels that were significant in any of the conditions.

Results

In the Task1 > Rest2 contrast of the PET data, there were significant clusters bilaterally in the frontal and posterior cingulate cortex and putamen, in the left orbitofrontal cortex, and in the right parietal cortex (Fig. 3 and Table 1).

In the corresponding contrast for the fMRI data, there were significant clusters mainly in the bilateral frontal, parietal, occipital, and cerebellar cortex (Supplemental Figure 1 and Supplemental Table 1–4). The fMRI clusters partly overlapped with those from PET in the frontal and parietal cortex (Fig. 4), also showing similar peak t-values (range 5.3 – 9.4 for PET; 5.6 – 12.9 for fMRI). The significant clusters tended to be smaller in the PET analysis than the spatially corresponding clusters in the task fMRI analysis. The FDG-PET clusters in the orbitofrontal cortex, putamen, and posterior cingulate cortex were not evident in the fMRI analysis. Conversely, fMRI indicated activations in cerebellum and visual cortex that were not evident in the PET analysis. Despite these mismatches, 53% of significant voxels in the PET analysis fell within significant clusters of the fMRI analysis. In the additional "contrast of contrast" analysis of the PET data, the above clusters were still present, but smaller in size (Supplemental Figure 2 and Supplemental Table 5).

Discussion

Using a standard clinical FDG-PET imaging protocol with single bolus injection, we were able to capture a pattern of WM task induced increase in relative FDG uptake at a group level. These relative increases were evident in regions known to be involved in WM (Nee et al., 2013; Owen et al., 2005; Rottschy et al., 2012; Swartz et al., 1995). The spatial pattern of the present FDG increases furthermore partly matched the results of our simultaneously acquired fMRI data. These findings suggest

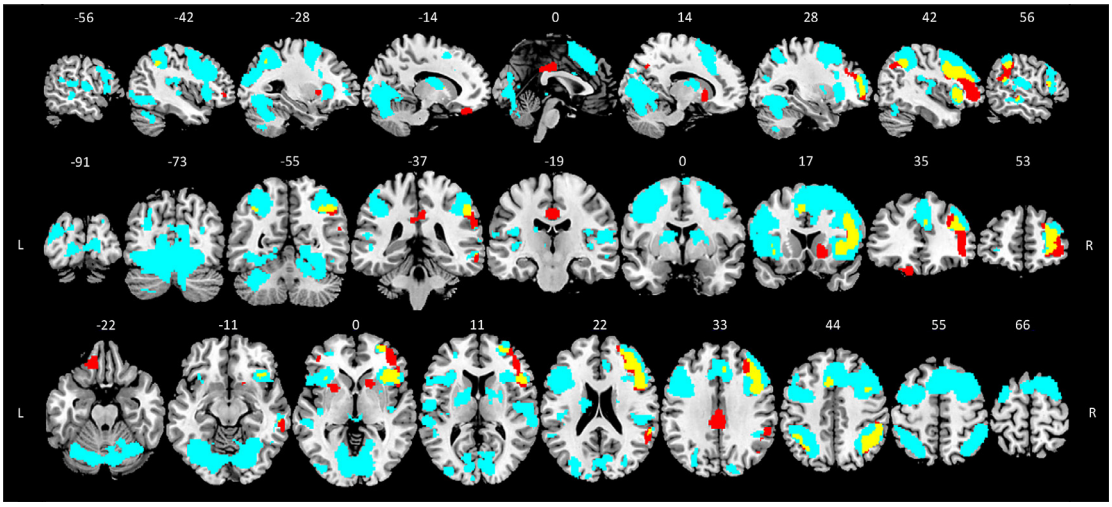

Fig. 4. Overlap between results in FDG-PET and fMRI data. Spatial overlap (yellow) of brain regions showing a significant task-induced change in globally normalized FDG uptake as measured with PET (red) and brain regions showing significant activations in single conditions of a WM task as measured with task fMRI (blue). L = left; R = right.

a potential of FDG-PET to delineate substrates of normal cognitive functions.

Of note, our experimental protocol was not designed to detect task-induced neural activity using FDG-PET, although the fMRI was perfectly fit for that task. Using a conventional bolus administration of 100 MBq FDG, we were able to detect relative increases in FDG uptake in a network of brain regions previously associated with WM performance. Indeed, approximately half of the voxels showing increased FDG uptake matched the voxels with WM-activation in the simultaneously acquired task fMRI data. These overlapping regions encompassed the frontal and parietal cortical regions belonging to the central executive network (Bressler and Menon, 2010; Fox et al., 2005). A recent meta-analysis of fMRI data highlighted critical engagement of this network in WM task processing (Emch et al., 2019). There was some mismatch of the patterns; the increased FDG uptake in posterior cingulate cortex, putamen, and orbitofrontal cortex did not overlap with fMRI activation. We note that the FDG uptake measured in the orbitofrontal cortex is vulnerable to spill-in from the nearby ocular muscles. On the other hand, the WM-task activation in the cerebellum and the visual cortex was present exclusively in the fMRI data. This disparity of PET results might stem from intrinsically lower glucose metabolism rate in these regions (Ishii et al., 2006, 2002), such that increases did not reach significance in the contrast of Rest2 and Test1 conditions. Still, the partial concordance with fMRI results supports the validity of the present FDG-PET findings as indicative of metabolic activation.

Although exciting, this interpretation calls for careful consideration of the assumptions implicit in our exploratory *ad hoc* analysis. In the clinical setting FDG-PET data acquisition commonly starts at 30 min p.i., but metabolic net trapping continues to approximately 90 min p.i., albeit at a progressively declining rate due to the depletion of the arterial input function. Due to the time-dependence of FDG uptake, the current guidelines recommend “a fixed time point for starting the acquisition (e.g. 30 min or 60 min after injection) to render the data from different patients or repeated scans comparable” (Varrone et al., 2009). As known from the earliest FDG-PET studies, the trapping of FDG in brain continues for hours, but at circulation times after 90 min p.i. the forward hexokinase reaction (k_3) is masked by the progressive dephosphorylation of FDG-phosphate (k_4), which could correspond to a binding potential of approximately 10 for gray matter in a steady-state condition (Huang et al., 1980). In conventional linear graphical analysis of FDG-PET data, the effect of k_4 is assumed to be negligible, but its contribution to the shape of the time-radioactivity curve in brain increases progressively (Tragardh et al., 2015). However, we confine our FDG-activation analysis to the intervals 52–60 min p.i. (Rest2), which was coincident with the resting state fMRI sequence, and the interval 63–71 min (Task1). Our procedure of global normalization will tend to have corrected for net trapping unrelated to the effects of activation. Furthermore, we performed an additional analysis with a correction for temporal changes in FDG uptake (Supplemental Figure 2 and Supplemental Table 5). We note that this correction is very conservative, as time-dependent increases in global FDG uptake have already been adjusted by the global normalization. That is to say, the Rest1, Rest2, and Task1 images were divided voxel-wise by whole brain FDG uptake (in SPM). Given the fewer degrees of freedom in this “contrast of contrasts”, the spatial extent of activated regions appeared to be smaller, but their persistence further supports our contention that we have isolated a pattern of metabolic activation due to task performance.

We acknowledge several limitations of the study. First, we did not quantify the metabolic rate of glucose relative to an arterial input function. Second, our results might be influenced by intrinsic regional differences in FDG uptake, thus emphasizing the apparent activations in neocortical regions.

We emphasize that we do not propose the present imaging protocol as a procedure to quantify cerebrometabolic activation by cognition. Admittedly, the effects were small and only evident to group analysis. Still, these results give evidence of the fitness of a single session PET recording after bolus FDG injection to detect neural activity due to a WM task, which motivates us to a dedicated FDG-PET imaging protocol for recording neural correlates of cognitive functions. Such a protocol should include a constant infusion of FDG by the time of a cognitive task to increase the sensitivity.

Competing interests

The authors declare that they have no conflict of interest.

Financial Support

This study was funded by the Deutsche Forschungsgemeinschaft (DFG) grant to KK [grant number KO 3744/8–1] and IY [grant number YA 373/3–1].

Data Availability

The data that support the findings of this study are available from the corresponding author on reasonable request. In this study all participants have signed an informed consent form approved by the local ethic committee stating that their data will only be made accessible to a third person for the purpose of clinical examination.

Code Availability

No new code was developed for generating the results. All results were obtained by functions belonging to publicly available software. The used software and/or functions are stated at appropriate location in the manuscript in the Methods section.

Author Contributions

I.R., L.W. and I.Y. contributed to the conception and design of the study. L.W. and I.R. analyzed together FDG-PET data. Q.W. analyzed together with I.R. and L.W. fMRI data. M.E. and I.R. recruited and tested participants. I.R., L.W. and I.Y wrote the manuscript in consultation with P.C. and K.K. All authors contributed to the manuscript revision and approved the submitted version.

Ethics statement

All procedures performed in studies involving human participants were in accordance with the ethical standards of the institutional and/or national research committee and with the 1964 Helsinki declaration and its later amendments or comparable ethical standards. Informed consent was obtained from all individual participants included in the study.

Acknowledgements

We thank Sylvia Schachoff, Claudia Meisinger, Anna Winter and Brigitte Mackert for their valuable assistance in scheduling and conducting of PET/MR examinations.

Supplementary materials

Supplementary material associated with this article can be found, in the online version, at doi:10.1016/j.neuroimage.2021.118131.

References

Bohnen, N.I., Djang, D.S., Herholz, K., Anzai, Y., Minoshima, S., 2012. Effectiveness and safety of 18F-FDG PET in the evaluation of dementia: a review of the recent literature. J. Nucl. Med. 53, 59–71.

Bressler, S.L., Menon, V., 2010. Large-scale brain networks in cognition: emerging methods and principles. Trends Cogn. Sci. (Regul. Ed.) 14, 277–290.

Delso, G., Furst, S., Jakoby, B., Ladebeck, R., Ganter, C., Nekolla, S.G., Schwaiger, M., Ziegler, S.I., 2011. Performance measurements of the Siemens mMR integrated whole–body PET/MR scanner. J. Nucl. Med. 52, 1914–1922.

Dukart, J., Bertolino, A., 2014. When structure affects function – The need for partial volume effect correction in functional and resting state magnetic resonance imaging studies. PLoS ONE 9, e114227.

Emch, M., von Bastian, C.C., Koch, K., 2019. Neural correlates of verbal working memory: an fMRI Meta-analysis. Front. Hum. Neurosci. 13, 180.

Fox, M.D., Snyder, A.Z., Vincent, J.L., Corbetta, M., Van Essen, D.C., Raichle, M.E., 2005. In: The Human Brain is Intrinsically Organized into Dynamic, Anticorrelated Functional Networks, 102. Proceedings of the National Academy of Sciences of the United States of America, pp. 9673–9678.

Hahn, A., Gryglewski, G., Nics, L., Hienert, M., Rischka, L., Vraka, C., Sigurdardottir, H., Vanicek, T., James, G.M., Seiger, R., Kautzky, A., Silberbauer, L., Wadsak, W., Mitterhauser, M., Hacker, M., Kasper, S., Lanzenberger, R., 2016. Quantification of task-specific glucose metabolism with constant infusion of 18F-FDG. Journal of Nuclear Medicine 57, 1933–1940.

Huang, S.C., Phelps, M.E., Hoffman, E.J., Sideris, K., Selin, C.J., Kuhl, D.E., 1980. Noninvasive determination of local cerebral metabolic rate of glucose in man. Am. J. Physiol. 238, E69–E82.

Ishii, K., Higashi, Y., Tabata, M., Miyaishi, M., Mizutani, T., Sasaki, M., 2006. Necessity of a uniform start for scanning after FDG injection in brain PET study. Ann. Nucl. Med. 20, 329–331.

Ishii, K., Sakamoto, S., Hosaka, K., Mori, T., Sasaki, M., 2002. Variation in FDG uptakes in different regions in normal human brain as a function of the time (30 and 60 min) after injection of FDG. Ann. Nucl. Med. 16, 299–301.

Jaeggi, S.M., Studer-Luethi, B., Buschkuehl, M., Su, Y.-F., Jonides, J., Perrig, W.J., 2010. The relationship between n-back performance and matrix reasoning — Implications for training and transfer. Intelligence 38, 625–635.

Jamadar, S.D., Ward, P.G., Li, S., Sforazzini, F., Baran, J., Chen, Z., Egan, G.F., 2019a. Simultaneous task-based BOLD-fMRI and [18-F] FDG functional PET for measurement of neuronal metabolism in the human visual cortex. Neuroimage 189, 258–266.

Jamadar, S.D., Ward, P.G.D., Carey, A., McIntyre, R., Parkes, L., Sasan, D., Fallon, J., Orchard, E., Li, S., Chen, Z., Egan, G.F., 2019b. Radiotracer administration for high temporal resolution positron emission tomography of the Human Brain: application to FDG-fPET. J. Vis. Exp..

Kim, S.G., Ogawa, S., 2012. Biophysical and physiological origins of blood oxygenation level-dependent fMRI signals. J. Cerebral Blood Flow Metabol. 32, 1188–1206.

Magistretti, P.J., Allaman, I., 2015. A cellular perspective on brain energy metabolism and functional imaging. Neuron 86, 883–901.

Nee, D.E., Brown, J.W., Askren, M.K., Berman, M.G., Demiralp, E., Krawitz, A., Jonides, J., 2013. A meta-analysis of executive components of working memory. Cerebral Cortex 23, 264–282.

Owen, A.M., McMillan, K.M., Laird, A.R., Bullmore, E., 2005. N-back working memory paradigm: a meta-analysis of normative functional neuroimaging studies. Hum. Brain. Mapp. 25, 46–59.

Phelps, M.E., Huang, S.C., Hoffman, E.J., Selin, C., Sokoloff, L., Kuhl, D.E., 1979. Tomographic measurement of local cerebral glucose metabolic rate in humans with (F-18)2-fluoro-2-deoxy-D-glucose: validation of method. Ann. Neurol. 6, 371–388.

Riedl, V., Utz, L., Castrillon, G., Grimmer, T., Rauschecker, J.P., Ploner, M., Friston, K.J., Drzezga, A., Sorg, C., 2016. In: Metabolic Connectivity Mapping Reveals Effective Connectivity in the Resting Human Brain, 113. Proceedings of the National Academy of Sciences of the United States of America, pp. 428–433.

Rischka, L., Gryglewski, G., Pfaff, S., Vanicek, T., Hienert, M., Klobl, M., Hartenbach, M., Haug, A., Wadsak, W., Mitterhauser, M., Hacker, M., Kasper, S., Lanzenberger, R., Hahn, A., 2018. Reduced task durations in functional PET imaging with [(18)F]FDG approaching that of functional MRI. Neuroimage 181, 323–330.

Rottschy, C., Langner, R., Dogan, I., Reetz, K., Laird, A.R., Schulz, J.B., Fox, P.T., Eickhoff, S.B., 2012. Modelling neural correlates of working memory: a coordinate-based meta-analysis. Neuroimage 60, 830–846.

Siebner, H.R., Peller, M., Willoch, F., Minoshima, S., Boecker, H., Auer, C., Drzezga, A., Conrad, B., Bartenstein, P., 2000. Lasting cortical activation after repetitive TMS of the motor cortex: a glucose metabolic study. Neurology 54, 956–963.

Swartz, B.E., Halgren, E., Fuster, J.M., Simpkins, E., Gee, M., Mandelkern, M., 1995. Cortical metabolic activation in humans during a visual memory task. Cerebral Cortex 5, 205–214.

Tragardh, M., Moller, N., Sorensen, M., 2015. Methodologic considerations for quantitative 18F-FDG PET/CT studies of hepatic glucose metabolism in healthy subjects. J. Nucl. Med. 56, 1366–1371.

Varrone, A., Asenbaum, S., Vander Borght, T., Booij, J., Nobili, F., Nagren, K., Darcourt, J., Kapucu, O.L., Tatsch, K., Bartenstein, P., Van Laere, K., European Association of Nuclear Medicine Neuroimaging, C., 2009. EANM procedure guidelines for PET brain imaging using [18F]FDG, version 2. Eur. J. Nucl. Med. Mol. Imaging 36, 2103–2110.

Verger, A., Guedj, E., 2018. The renaissance of functional (18)F-FDG PET brain activation imaging. Eur. J. Nucl. Med. Mol. Imag. 45, 2338–2341.

Villien, M., Wey, H.Y., Mandeville, J.B., Catana, C., Polimeni, J.R., Sander, C.Y., Zurcher, N.R., Chonde, D.B., Fowler, J.S., Rosen, B.R., Hooker, J.M., 2014. Dynamic functional imaging of brain glucose utilization using fPET-FDG. Neuroimage 100, 192–199.